The International Journal of Advanced Manufacturing Technology
https://doi.org/10.1007/s00170-026-17877-1

ORIGINAL ARTICLE

An industry-oriented workflow for noise reduction in handheld 3D scanning: A case study in automated dimensional inspection

Scott Robinson[1] · Chengsi Lin[1] · Muhamad Arfauz A Rahman[1] · Paul G. Maropoulos[2] · Effendi Mohamad[2] · Teruaki Ito[3]

Received: 20 October 2025 / Accepted: 11 March 2026

Abstract

Reliable dimensional inspection with handheld 3D scanners is frequently affected by unstable environmental conditions, reflective surfaces, and operator-dependent variability. This study introduces a practical, industry-oriented workflow designed to minimize noise during both acquisition and post-processing. The approach combines controlled lighting and temperature management, surface preparation using matte spray coatings, and optimized scanning trajectories to enhance data capture stability. These acquisition strategies are followed by a structured post-processing pipeline in Artec Studio 17, emphasizing targeted noise filtering while preserving small geometric features. Three machined components of differing complexity were evaluated, with dimensional accuracy assessed against their corresponding CAD models. The proposed workflow yielded average improvements of 1–2% in geometric fidelity and reduced variability across repeated scans. While the method relies on commercial software, it offers clear industrial value by improving inspection consistency, lowering rework rates, and supporting more efficient metrology practices. The findings provide actionable guidance for manufacturers seeking practical, workflow-based solutions for noise reduction in handheld 3D scanning environments.

Keywords Artec Leo · Quality control · Noise reduction · Workflow optimization

1 Introduction

Quality control is essential in manufacturing to ensure products meet performance, safety, and dimensional specifications [1]. Traditional inspection methods—such as manual measurements using digital calipers, micrometers, and coordinate measuring machines (CMMs)—depend heavily on operator skill and equipment calibration [2]. These approaches are prone to human error and calibration drift, which can result in costly quality failures [3]. For instance, the Williams F1 team was disqualified from qualifying for the 2024 Dutch Grand Prix due to an oversized floor body caused by miscalibrated measurement tools [4], while Boeing grounded 171 aircraft in January 2024 after a door plug failure linked to missed fasteners during manual inspection [5].

To mitigate such risks, manufacturers are increasingly integrating digital inspection technologies under the Industry 4.0 framework [6]. Automated and optical 3D scanning systems enhance accuracy, reduce inspection time, and minimize operator dependence. For example, ScanTECH and NIKI Rotor Aviation implemented a 3D scanning solution for aircraft door alignment, achieving 0.025 mm accuracy and reducing inspection time to 10 min [7]. Similarly, Andritz Hydro reduced setup time for turbine blade inspection from two days to two hours by adopting handheld 3D scanning [8].

Despite these benefits, challenges remain in ensuring scan accuracy under real-world conditions. Key issues include ambient light variation, surface reflectivity, point cloud alignment, and limited detection of small geometric features. These factors contribute to noise—positional deviations between the scanned point cloud and the true surface geometry [9]. In dimensional inspection, noise can obscure critical features and reduce measurement reliability. A study by the University of Stavanger [10] reported significant

✉ Chengsi Lin
clin08@qub.ac.uk

1 Queen's University Belfast, Belfast, UK

2 Universiti Teknikal Malaysia Melaka, Melaka, Malaysia

3 Faculty of Business Administration, Matsuyama University, Matsuyama, Japan

surface irregularities and an average dimensional error of 0.113 mm in a cylindrical component scan, highlighting the impact of noise on measurement fidelity, as shown in Fig. 1.

Post-processing to remove such noise often dominates total inspection time, as shown in a University of Uludag study where point cloud refinement accounted for 94.9% of the total process despite achieving 0.1 mm tolerance accuracy [11]. Although numerous denoising algorithms have been proposed, most are developed under ideal laboratory conditions assuming Gaussian noise distributions, limiting their robustness in industrial settings where noise sources are complex and variable.

Despite the extensive availability of noise reduction techniques for point clouds, most existing studies focus on algorithmic development under laboratory or simulated conditions, often assuming stationary scanners, controlled illumination, and Gaussian noise distributions. In contrast, noise in handheld structured-light scanning arises from a complex coupling between optical physics, operator motion, surface reflectivity, and feature geometry, making direct application of state-of-the-art denoising algorithms impractical for industrial inspection contexts. The primary contribution of this work is not the proposal of a new denoising algorithm, but the systematic investigation of noise controllability within the physical and operational constraints of handheld structured-light scanners. This study introduces a two-stage, inspection-oriented framework that explicitly links noise sources to geometric feature classes and evaluates how acquisition-level and post-processing interventions influence dimensional accuracy at both global and local scales.

Unlike existing workflow descriptions or vendor guidelines, this research provides quantitative evidence of how different noise mitigation strategies affect feature-dependent measurement fidelity, particularly highlighting the limited effectiveness of global smoothing for small, recessed, or high-curvature features. Through controlled experiments on industrial components of increasing geometric complexity, this work clarifies the boundary between removable noise and irrecoverable information loss imposed by optical resolution, occlusion, and reflectivity effects. By reframing noise reduction as a constraint-aware inspection problem rather than a purely computational task, this study contributes new insight into the realistic performance limits of handheld 3D scanning in automated dimensional inspection, thereby bridging the gap between academic noise reduction research and industrial metrology practice.

2 Literature review

2.1 Overview of 3D scanning technology

3D scanning is a rapid, non-contact method used to capture the geometry of physical objects and represent them digitally with high surface fidelity [12]. Although 3D scanning technologies date back to the 1960s [13], advancements have led to four primary methods: laser triangulation, photogrammetry, LiDAR (Light Detection and Ranging), and structured light systems (SLS) [2]. Among these, SLS offers the best balance of accuracy, speed, and ease of use for metrology, reverse engineering, and quality control [9]. Structured light scanners project a light pattern onto an object and capture its distortion using cameras to calculate precise 3D coordinates through triangulation, as shown in Fig. 2 [14]. This technique enables rapid, high-resolution data collection (up to 750,000 points per second) without requiring specialist metrology expertise [5, 7, 15].

2.2 Sources of noise in 3D scanning

Despite their advantages, structured light scanners are highly sensitive to environmental, material, and setup factors that introduce **noise**—unwanted deviations between

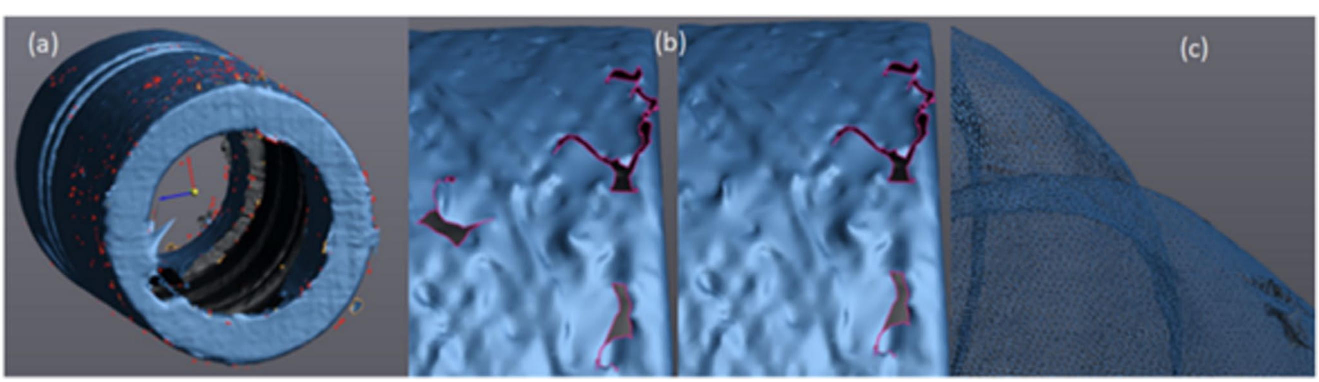

Fig. 1 Noise obtained from 3D scanning hindering geometric measurements [10]

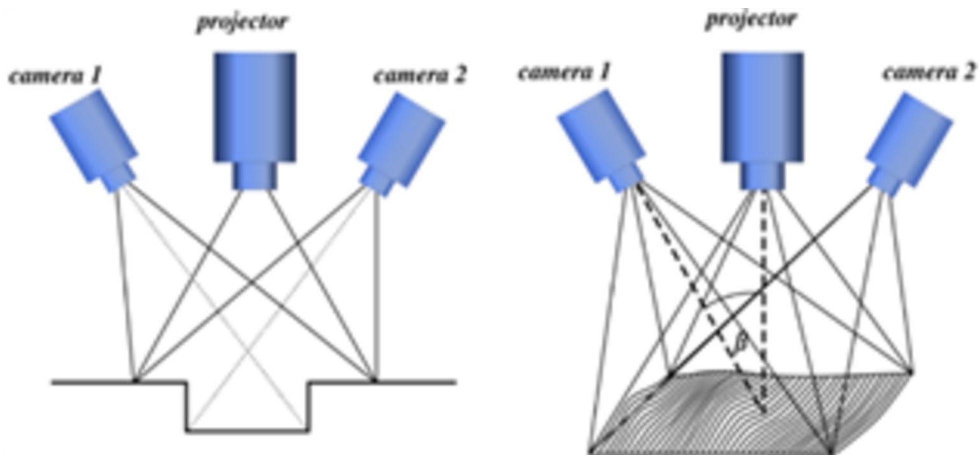

Fig. 2 Complexity branch diagram [14]

Table 1 Effects of surface properties on 3D Scanning summarised [25]

Surface Properties	Influence on Scanner Light	Effect on cloud point data	Effect on final model
Transparent/Clear	Light moves through the surface	Will not capture the surface	No model generated
Reflective/Shiny	Light scatters in uncontrolled directions	Generate high levels of noise or ghost point	Inaccurate measurements of geometric features
Monochromatic, Low Contrast or Repetitive patterns	Scanner unable to distinguish between surfaces.	Sparse point clouds	Inaccurate measurements of geometric features
Dark/Black	Absorbs emitted light	Sparse point clouds	Inaccurate measurements of geometric features

captured points and the true surface. Tingcheng Li et al. [9] identified key influences including ambient lighting, surface reflectivity, and scanner configuration, but comprehensive studies on their combined effects remain limited. Noise sources can be grouped into three categories:

- **Environmental factors**: ambient light and temperature gradients.
- **Object properties**: surface reflectivity, colour, and texture.
- **Scanner parameters**: configuration, scanning path, and distance.

These factors often interact; for example, bright lighting on reflective surfaces amplifies measurement distortion. Understanding such interactions is essential for developing robust industrial scanning procedures.

2.2.1 Environmental factors

Uniform lighting is more critical than intensity alone—tests at 0, 280, and 660 lx showed no significant accuracy change (< 0.066 mm), but inconsistent illumination introduced random error [16]. Similarly, temperature gradients affect both air density and material dimensions; a 2 °C variation can induce a 0.025 mm error at 5 m range [17]. Industrial inspection standards therefore recommend controlled environments at 20 °C to minimize thermal distortion [18].

2.2.2 Object surface properties

Surface reflectivity remains a major noise contributor [10, 19, 20]. Specular reflections cause "ghost points" and "edge flares" near concave and sharp features [21, 22]. Surface treatments such as matte or anti-glare sprays can mitigate reflections with minimal dimensional impact (e.g., AESUB spray, 0.007 mm layer thickness) [23]. Path planning also affects reflection-induced noise; adjusting scanning angles and using zig-zag trajectories can significantly reduce outliers on metallic parts [24].

Surface colour and texture influence light absorption and scattering. Dark or transparent materials often yield sparse or incomplete point clouds, while repetitive or low-contrast textures confuse tracking systems, as shown in Table 1.

2.2.3 Scanner setup

Field of view (FOV) limitations prevent capturing recessed or internal features, such as holes or threads, as shown in Fig. 3 [26]. Moreover, scanning distance significantly affects accuracy; Sun et al. [27] observed noise increasing from 30 µm at 585 mm to 80 µm at 1200 mm. Maintaining consistent and optimal scanner-to-object distance is therefore crucial in industrial workflows.

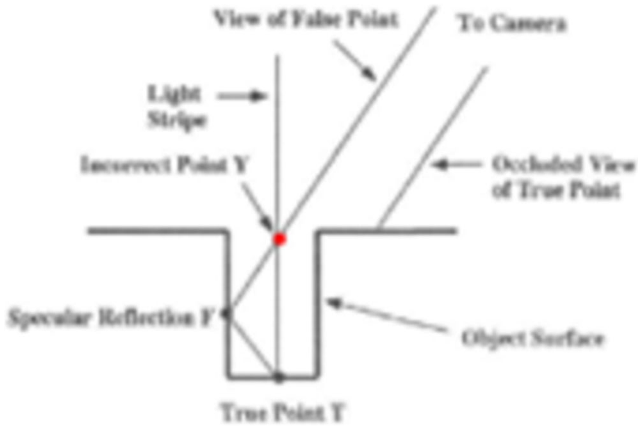

Fig. 3 FOV challenges when 3D scanning a hole [26]

2.3 2.3 Noise reduction techniques

Noise in point clouds complicates downstream inspection and measurement, prompting development of numerous denoising techniques broadly classified as filtering, optimisation, and machine learning approaches [28]. Filtering methods, such as Statistical Outlier Removal (SOR) and bilateral filtering, rely on mathematical thresholds to identify and remove irregular points [29–32]. These are simple and computationally efficient but highly dependent on user-defined parameters and can inadvertently remove valid data. Optimisation-based methods, like Moving Least Squares (MLS), reconstruct smooth surfaces by fitting local polynomials to data points [33–35]. While effective at reducing noise and preserving overall shape, these methods are computationally intensive and tend to over-smooth critical features, limiting their practicality for large industrial datasets. Machine learning and deep learning methods (e.g., PointNet, PointCleanNet) have demonstrated strong denoising potential in research environments [36, 37]. However, they require extensive training data, high computational power, and are rarely validated on handheld scanners in real-world conditions. Their "black box" nature also limits industrial adoption in regulated sectors such as aerospace and healthcare.

Overall, existing noise reduction research is predominantly theoretical or lab-based, with limited validation in dynamic, handheld industrial contexts. Deep learning and optimisation methods, while accurate, are resource-heavy and impractical for battery-powered portable scanners. This highlights a clear gap between academic research and industrial application, where a validated, efficient, and operator-friendly workflow for handheld 3D scanning is urgently needed.

Although numerous filtering, optimisation, and learning-based denoising methods have been proposed, their evaluation is predominantly conducted on synthetic datasets or static scans, with limited consideration of handheld operation, feature-level inspection accuracy, or industrial time and resource constraints. Consequently, there is a lack of empirical understanding regarding which types of noise are practically reducible in handheld structured-light scanning and which errors fundamentally persist due to physical and geometric limitations.

2.4 2.4 Fundamentals of point cloud processing

Point clouds represent surfaces as discrete 3D coordinates (x, y, z) [38], which can be enhanced with colour and normal data for improved realism. Surface reconstruction typically converts point clouds into mesh formats such as STL or B-Rep for CAD comparison [39]. However, raw point clouds often contain uneven densities and two primary noise types: outliers (isolated, erroneous points) and random noise (minor surface roughness deviations) [2]. Both degrade dimensional accuracy by distorting surface geometry and masking small features. As illustrated in Fig. 4, these noise types are defined by positional deviation from the true surface [40]. While statistical methods can detect

Fig. 4 Example of 3D point cloud noise [40]

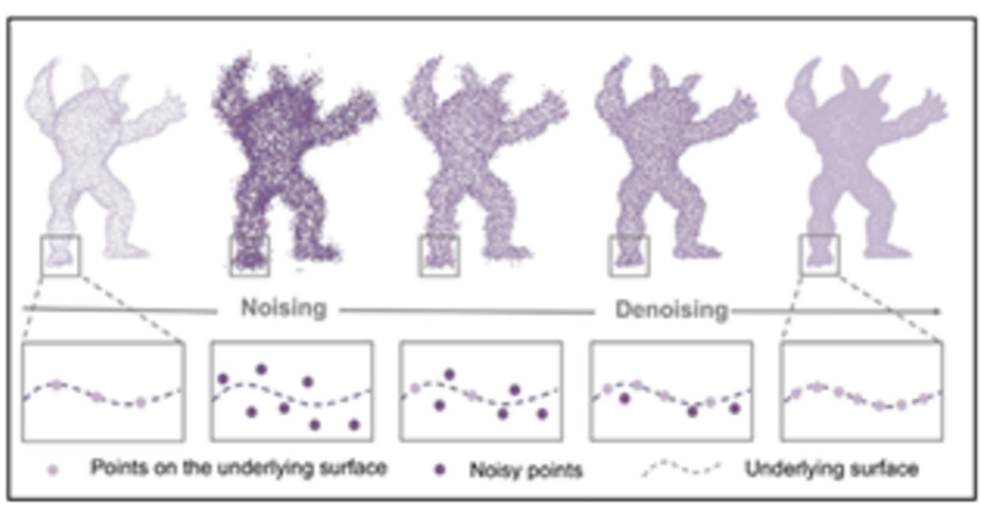

such deviations using mean (μ) and standard deviation (σ) boundaries [5], real-world noise rarely follows ideal distributions, reinforcing the need for practical, empirically validated approaches.

3 3. Methodology

Although the individual components of the proposed workflow—such as surface treatment, environmental stabilization, optimized scanning paths, and software-based filtering—have been discussed separately in prior studies, their combined influence on dimensional inspection accuracy has not been systematically evaluated. This study introduces a structured, two-stage methodology that explicitly distinguishes between acquisition-stage noise suppression and post-processing noise attenuation.

The methodological contribution of this work is threefold:

- Provides a reproducible framework that formalizes best-practice scanning procedures into an experimentally verifiable workflow.
- Quantitatively evaluates the marginal and cumulative effects of each stage on global and feature-level accuracy.
- Interprets the observed improvements in the context of optical resolution limits and metrological reliability.

By shifting the focus from algorithmic optimality to inspection robustness, the proposed methodology contributes a complementary perspective to existing denoising research.

3.1 3D scanning process

As shown in Fig. 5, data acquisition was performed using the Artec Leo 3D Scanner, a handheld structured light scanner designed for industrial-grade metrology applications. The device employs a white LED array and captures 3D geometry at up to 80 FPS within a 0.35–1.2 m working range, delivering point accuracy of 0.1 mm and resolution of 0.2 mm. Unlike simulated or public datasets, this study prioritised real-world noise conditions typical of manufacturing environments to evaluate the robustness of handheld 3D scanning. And the scanning process followed the workflow shown in Fig. 6, ensuring consistency, traceability, and repeatability.

All scans were conducted in a controlled laboratory environment maintained at 20 ± 0.5 °C, as shown in Fig. 7, replicating standard inspection room conditions to minimise thermal distortion [4]. Calibration ensured stable capture parameters at an optimal 0.5 m working distance, limiting scanning speed to 60 FPS to prevent motion blur. Each aluminium workpiece was cleaned, marked with at least three alignment points, and positioned against a contrasting background. The operator followed a slow, circular scanning path at a 45° angle, maintaining consistent distance and orientation while monitoring the real-time quality map on the scanner display. Each dataset comprised approximately 800–1200 frames across two orientations to ensure full coverage.

These conditions were intentionally selected to isolate the effects of the proposed noise reduction workflow from external disturbances. As a result, the present study does not

Fig. 5 Artec Leo 3D Scanner

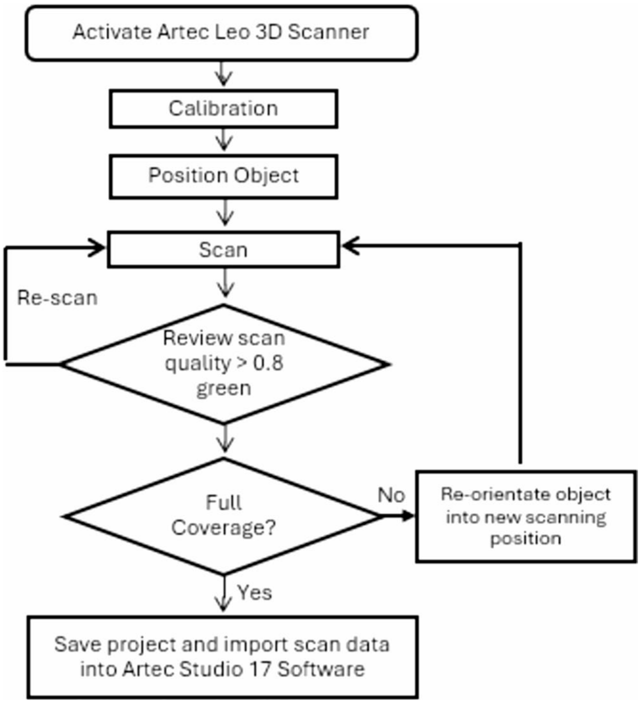

Fig. 6 3D scanning process flowchart

aim to replicate the full variability of factory-floor environments, but rather to establish a controlled performance baseline against which future robustness-oriented investigations may be compared.

Table 2 Summary of products used for scanning

Product name	Image	Geometric Features
Base Block	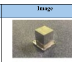	• Sharp Edges and Corners • Chamfers • Threaded Holes • Notches
Fixture		• Steps • Slot • Fillets • Blind Holes
Fastener	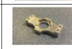	• Sharp Edges and Corners • Pockets • Curvatures • Fillets • Blind & Through Holes

3.2 Scanned products-prepare

Three machined aluminium components were selected to represent varying geometric complexity and reflectivity, as shown in Table 2. Aluminium's reflectivity posed a significant challenge for structured-light scanning; therefore, a thin, uniform layer of white matte scanning spray (Bastille) was applied at a 30 cm distance to reduce local reflections and scattering, as shown in Fig. 8. This temporary coating enhanced surface uniformity without altering part geometry, supporting sustainability through residue-free removal and component reusability.

Images of measurements of all products can be found in Appendix *A*, as well as engineering drawings in Appendix *B* with extended details of dimensions.

3.3 Accuracy and improvement evaluation

Scan accuracy was quantified by the Root Mean Square Error (RMSE) between the point cloud and reference CAD model, as shown in Eq. 1:

Fig. 7 Light and temperature levels measured in the research laboratory

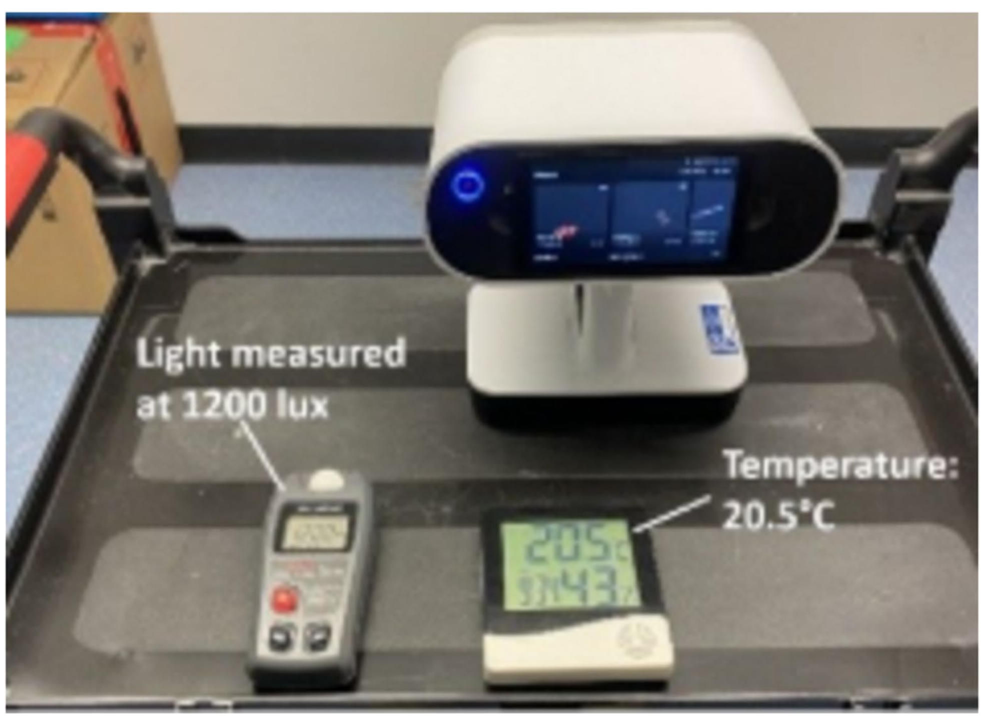

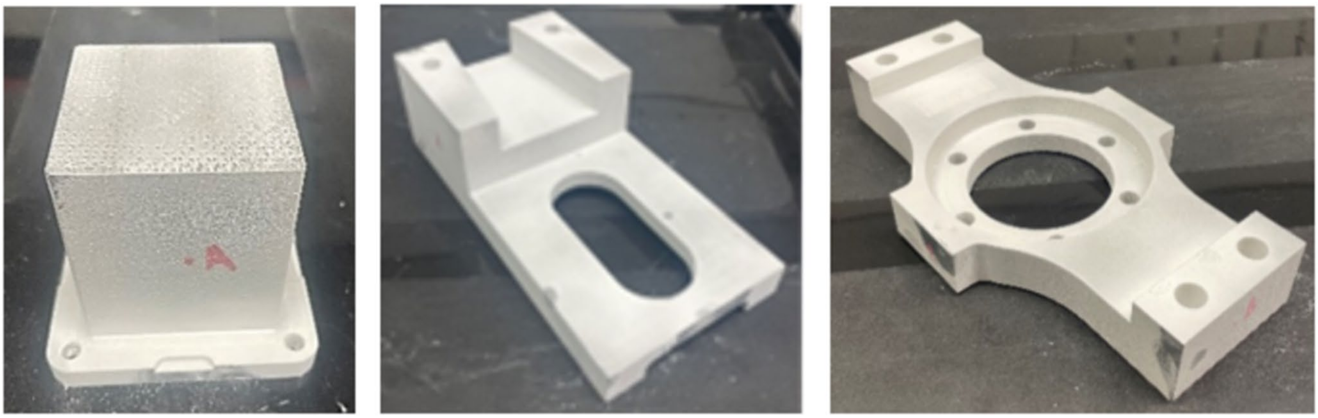

Fig. 8 Matte coating applied to workpieces

Fig. 9 Flowchart of proposed methodology for noise reduction

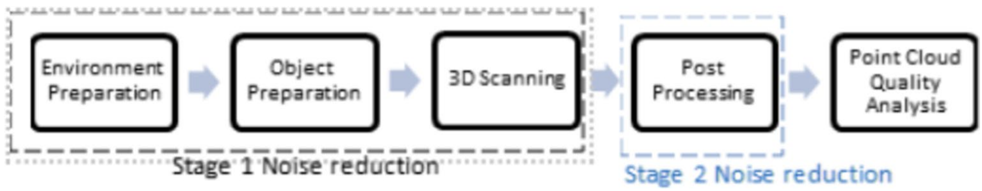

$$RMSE = \sqrt{\frac{1}{n}\sum_{i=1}^{n}\left(\bar{x}_i - x_i\right)^2}$$

Eq. 1. Root Mean Square Error

where $x_i^{\prime}$ and x_i represent corresponding points on the scanned and reference models. This provides an objective, repeatable metric for evaluating accuracy improvements across different workflow stages.

The effectiveness of these interventions was evaluated through dimensional accuracy relative to actual physical measurements of the products, computed as Eq. 2:

$$Accuracy\,(\%) = \left(1 - \left|\frac{MeasurementDimension - ScanDimension}{MeasurementDimension}\right|\right) * 100$$

Eq. 2. Accuracy

Accuracy improvement against actual physical measurements from initial noise identification to post Stage one (%) was calculated by Eq. 3:

$$AccuracyImprovement\,(\%) = NoiseIdentificationAccuracy\,(\%) - AccuracyAfterStageOne\,(\%)$$

Eq. 3. Accuracy Improvement

3.4 Noise reduction

The proposed workflow shown in Fig. 9 integrates noise reduction measures into two complementary phases—during scanning and post-processing—to minimise deviation and enhance geometric fidelity. During scanning, environmental control, matte surface coating, and optimised scanning paths were applied to reduce optical noise and occlusions.

Subsequent post-processing was carried out in Artec Studio 17, following a consistent alignment and cleaning protocol to enhance reproducibility. And to improve reproducibility and facilitate adoption by the wider research community, the key processing operations were defined in terms of algorithmic function and parameter ranges rather than software-specific implementations. Scans were first cropped to remove extraneous data, then aligned using a combination of pair-point registration, rough, fine, and global registration. Global registration parameters were tuned to a key frame ratio of 0.5 and a feature search radius of 0.6 mm, balancing accuracy with computational efficiency. Scans exceeding a maximum registration error of 0.5 were excluded to ensure measurement reliability.

the outlier removal step applied in Artec Studio corresponds to a statistical neighbourhood-based filtering strategy, conceptually equivalent to Statistical Outlier Removal (SOR) commonly implemented in open-source libraries such as the Point Cloud Library (PCL) and CloudCompare. In this study, a threshold of 2–3 standard deviations (σ) were used to identify and remove isolated points, which aligns with parameter ranges reported in prior point cloud denoising literature.

The smooth fusion algorithm was selected for mesh reconstruction, as it produced the most balanced results between surface uniformity and preservation of detail, compared to the fast and sharp fusion alternatives, as shown in

Fig. 10. This can be approximated by Moving Least Squares (MLS) surface reconstruction methods available in open-source platforms. Both approaches rely on fitting local polynomial surfaces to neighbourhoods of points to suppress high-frequency noise while preserving low-frequency geometric structure. To ensure comparability, neighbourhood radii between 0.3 mm and 0.6 mm were selected based on the scanner's nominal resolution and average point spacing.

To further enhance coverage and mitigate occlusions, multi-scan integration was implemented, combining two, four, and eight scans per workpiece. Increased scan counts improved surface completeness and reduced localised noise, resulting in measurable RMSE reductions and greater geometric consistency. While processing times increased with scan quantity, the improvement in model fidelity demonstrated the practical trade-off for industrial inspection scenarios.

Overall, the developed workflow offers a repeatable, operator-friendly, and sustainable process for handheld 3D scanning in industrial contexts. By combining controlled acquisition, physical surface treatment, and structured post-processing, it enables robust dimensional inspection with reduced noise sensitivity—without requiring complex algorithmic filtering or machine learning methods. Future work will explore integration with AI-assisted denoising and automated defect detection to further streamline digital inspection pipelines for manufacturing applications.

4 Results

4.1 Noise identification in workpieces

The noise characteristics of the scanned workpieces were first evaluated by importing the raw point clouds into Artec Studio 17 and generating polygonal meshes to visualise error distribution. The base block exhibited random noise concentrated around sharp corners due to mixed light reflections and scattering (Fig. 11c). Mirror-finished interfacing surfaces generated multipath reflections, producing bridged noise between boundaries and obscuring small features such as threaded holes and notches (Fig. 11b). The resulting deviations yielded an RMSE of 0.340 mm and MAE of 0.298 mm relative to the CAD reference.

The fixture showed similar noise behaviour, with step boundaries producing multipath reflections and random bridging between surfaces (Fig. 12b). Stepped features also restricted the scanner's field of view, leading to occlusions that required multiple orientations to capture hidden geometry. Oval noise patterns were visible around slots, likely caused by inconsistent scanning motion, while concave fillets introduced outliers from light scattering (Fig. 12c). The RMSE and MAE were 0.323 mm and 0.308 mm, respectively.

The fastener, with its complex pockets, fillets, holes, and sharp edges, exhibited the most severe noise artefacts. Occluded regions outside the scanner's field of view resulted in sparse point clouds (Fig. 13c), and reflective step boundaries caused undefined edges. Blind and through holes were poorly reconstructed due to unfavourable angles and limited illumination, with recessed areas showing shadow-induced noise. The RMSE and MAE were 0.618 mm and 0.599 mm, respectively, confirming that geometric complexity and reflectivity amplify noise generation during handheld scanning.

4.2 Effectiveness of stage one: Pre-processing noise reduction

Stage one of the workflow focused on physical noise mitigation through matte surface coating, environmental control, and optimised scanning paths. These measures collectively reduced multipath reflections and surface glare, leading to more stable data acquisition. Dimensional accuracy, evaluated per Eq. 1, improved across all workpieces, as shown in Table 3.

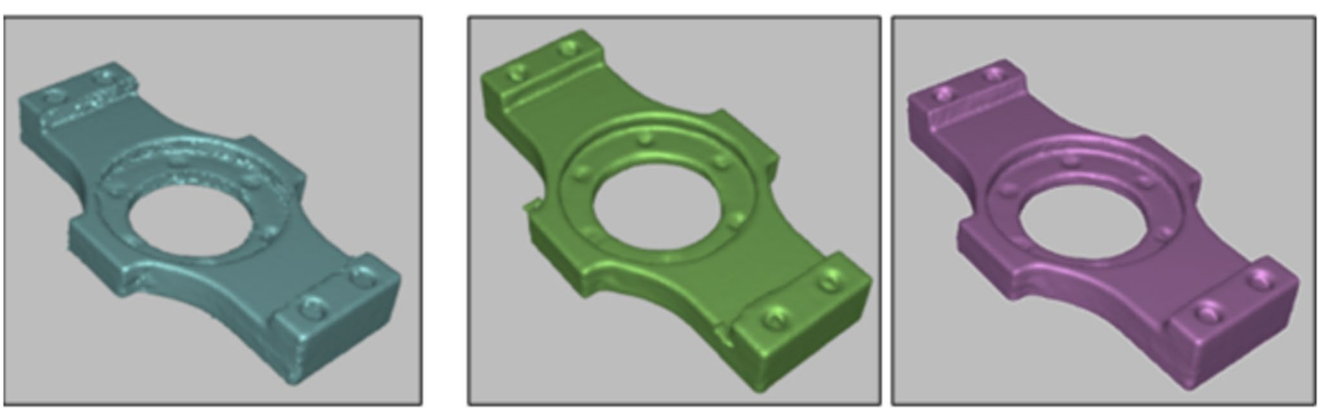

Fig. 10 (**a**) Fast fusion (left), (**b**) Sharp fusion (middle), (**c**) Smooth fusion (right)

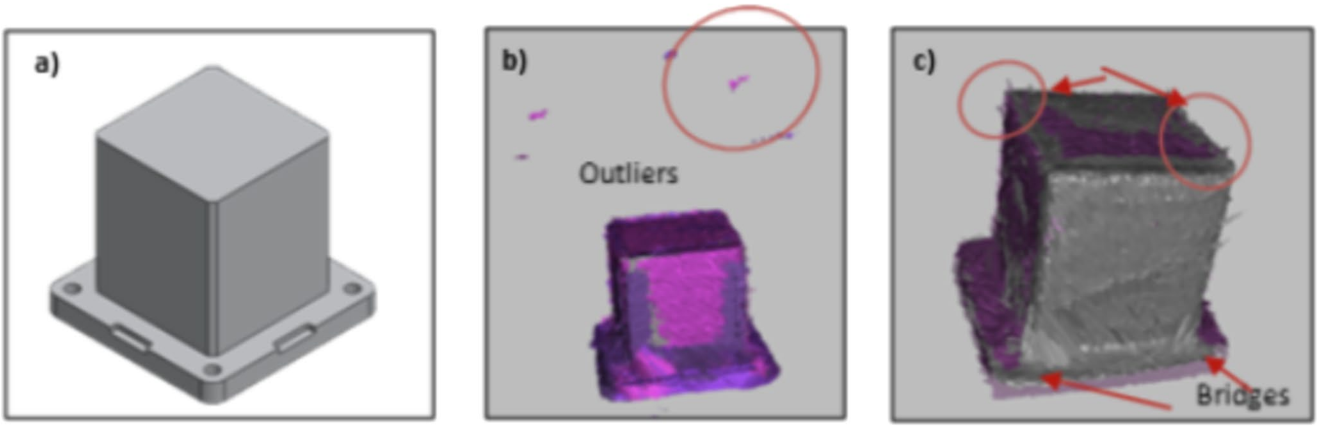

Fig. 11 (**a**) Base Block Ground Truth; (**b**) Scan 1: Outliers; (**c**) Scan 2: Random Noise

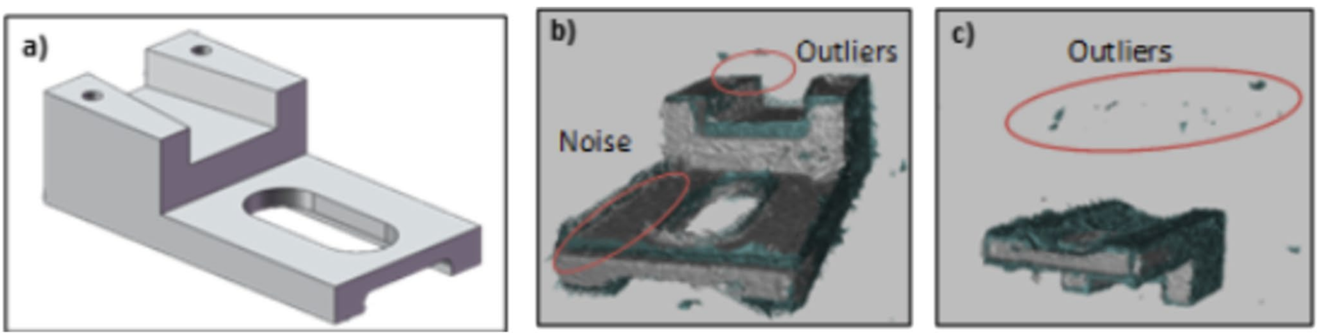

Fig. 12 (**a**) Fixture Ground Truth; (**b**) Scan 1; (**c**) Scan 2

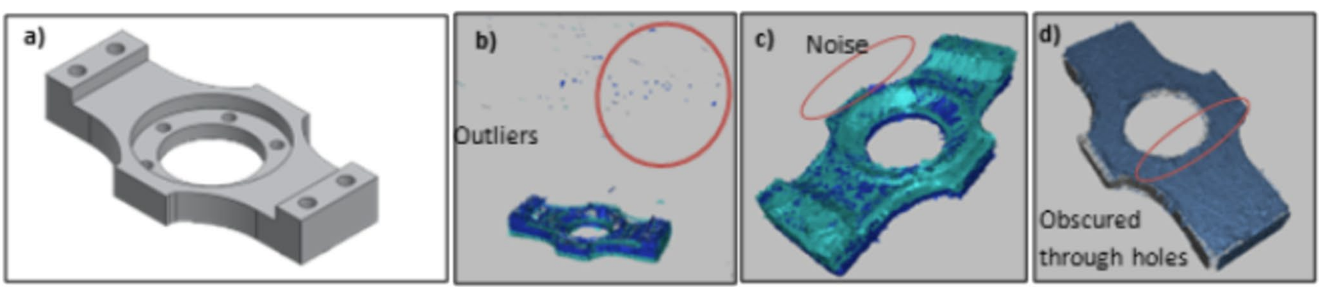

Fig. 13 (**a**) Fastener Ground Truth; (**b**) Scan 1; (**c**) Scan 2; (**d**) Scan3

The base block and fixture achieved overall accuracy improvements of 0.90% and 0.53%, respectively, while the fastener—the most geometrically complex—showed a more significant increase of 1.79%. Local improvements were most notable in the fixture's step width (+4.15%), though some features such as hole diameter and slot length showed marginal losses (−0.40% and −0.12%, respectively). On average, dimensional accuracy increased by 1.03%, confirming that pre-processing effectively reduced reflection-induced noise. However, minor deviations persisted, particularly around small and recessed features, necessitating further digital post-processing.

4.3 Comparison of smoothing techniques

4.3.1 Base block

Smoothing algorithms within Artec Studio 17 were applied to evaluate post-processing effects on geometric accuracy. For the base block (Fig. 14), sharp fusion at 0.3 mm resolution maintained edge definition but introduced minor shrinkage along primary dimensions (Width 1 = 49.42 mm; Width 2 = 49.81 mm). Small-scale noise obscured the measurement of small features prior to smoothing preventing a full assessment as seen Table 4. The RMSE and MAE

Table 3 Stage one pre-processing scans of the workpieces

Product	Top Orientation	Bottom Orientation
Fixture		
Fastener		
Based block		

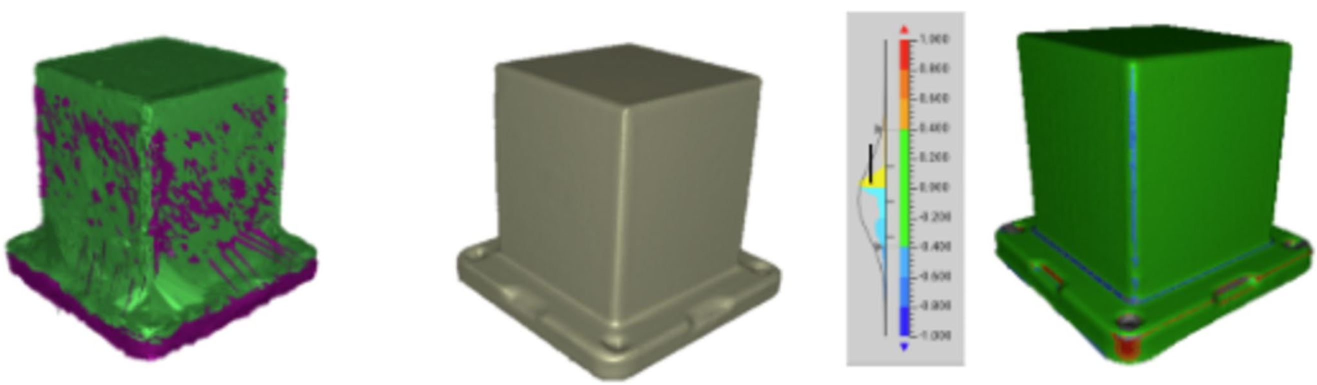

Fig. 14 Base block before smoothing (left), after smoothing (middle), Surface deviation map (right)

improved to 0.238 mm and 0.177 mm, respectively, reflecting reduced random noise. While smoothing improved large planar surfaces, small-scale features such as threaded holes and notches remained difficult to measure accurately (84.80% and 53.00%), indicating that excessive smoothing can obscure fine details.

4.3.2 Fixture

For the fixture (Fig. 15), smooth fusion with 0.5 mm resolution achieved the best balance between detail preservation and noise reduction, producing an RMSE of 0.305 mm and MAE of 0.301 mm. Large geometric features such as width, step length, and slot dimensions achieved accuracies above 99%, demonstrating the algorithm's suitability for prismatic components. However, smaller features such as hole diameter (95.90%) and unmeasurable hole depth highlighted the continuing limitation of smoothing for recessed geometries, as seen in Table 5 posed challenges.

4.3.3 Fastener

The fastener presented the most demanding test for smoothing algorithms due to its complex geometry (Fig. 16).

Table 4 Dimension analysis of the impact of smoothing on the base block model

Dimension	CAD (mm)	Actual physical measurements	Before Smoothing (mm)	After Smoothing (mm)	Accuracy against measurement after smoothing (%)	Smoothing Accuracy Improvement (%)
Width 1 (mm)	50	49.97	50.14	49.42	98.90	-0.76
Width 2 (mm)	50	50.01	50.64	49.81	99.60	0.86
Height (mm)	62.5	62.54	63.27	62.67	99.79	0.96
Height-Base (mm)	55	55.00	55.21	55.00	100	0.38
Base Depth (mm)	7.5	7.55	N/A	7.78	97.04	N/A
Threaded Hole Diameter (mm)	5	5.12	5.94	5.76	87.5	3.52
Notch Depth (mm)	2	2.06	N/A	2.94	57.28	N/A
Notch Length (mm)	15	14.99	N/A	14.64	97.67	N/A

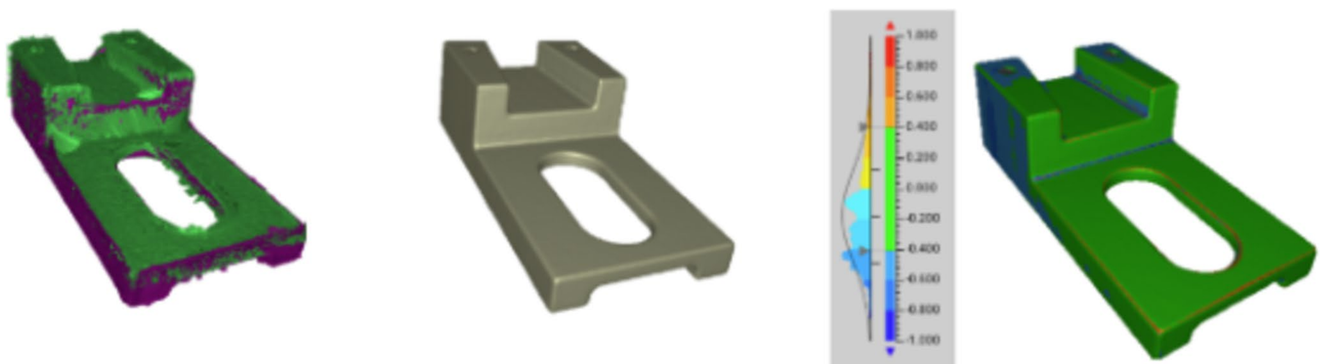

Fig. 15 Fixture before smoothing (left), after smoothing (middle), Surface deviation map (right)

Table 5 Dimension analysis of the impact of smoothing on the fixture model

Dimension	CAD (mm)	Actual physical measurements	Before Smoothing (mm)	After Smoothing (mm)	Accuracy against measurement after smoothing (%)	Smoothing Accuracy Improvement (%)
Width (mm)	100	100.04	101.25	100.38	99.66	0.87
Step Length (mm)	80	80.10	80.77	80.26	99.80	0.64
Step Depth (mm)	60	60.12	60.66	60.45	99.45	0.35
Hole Dia (mm)	10	9.97	9.49	9.59	96.19	1.00
Hole Depth (mm)	20	20.06	N/A	N/A	N/A	N/A
Slot Width (mm)	40	39.85	38.94	40.25	98.90	1.18
Slot Length (mm)	90	89.90	88.61	90.03	99.86	1.31
Groove Width (mm)	60	59.98	59.41	60.23	99.58	0.53
Groove Depth (mm)	10	10.11	10.85	9.96	98.52	5.84

Smooth fusion at 0.3 mm resolution yielded an RMSE of 0.457 mm and MAE of 0.514 mm, representing a notable improvement over raw scans. Key dimensions such as width and pocket diameters achieved accuracies exceeding 99%, while smaller features like step depth (97.23%) and hole diameter (95.70%) were less consistent highlighted challenges in preserving fine features as seen in Table 6. Overall, smoothing improved step width by 5.65% and step length by 2.62%, confirming its effectiveness for large or complex surfaces but revealing trade-offs between noise removal and small-feature fidelity.

Across all workpieces, smoothing enhanced average dimensional accuracy by 1.76%, demonstrating consistent improvement. However, from an industrial perspective, over-smoothing risks losing fine detail crucial for inspection of precision components, highlighting the need for adaptive smoothing strategies that preserve small geometries while minimising noise on larger surfaces.

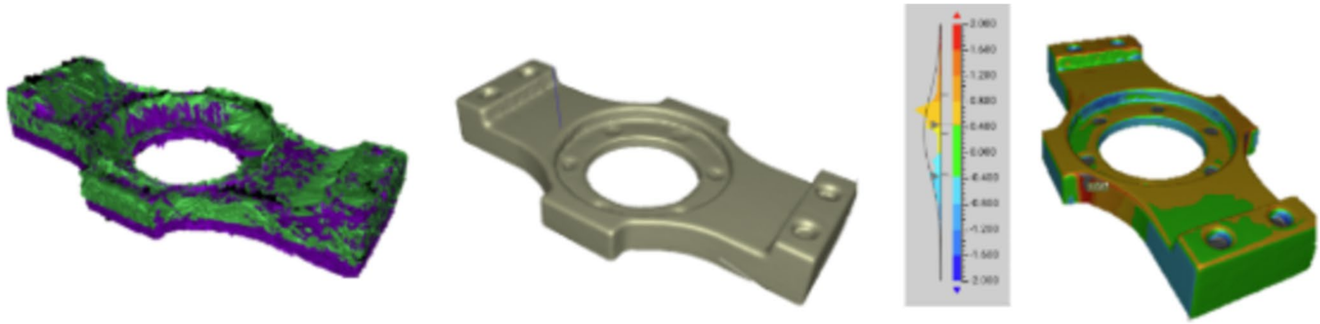

Fig. 16 Fastener before smoothing (left), after smoothing (middle), Surface deviation map (right)

Table 6 Dimension analysis of the impact of smoothing on the fastener model

Dimension	CAD (mm)	Actual physical measurements	Before Smoothing (mm)	After Smoothing (mm)	Accuracy against measurement after smoothing (%)	Smoothing Accuracy Improvement (%)
Width (mm)	112.37	112.39	115.03	112.51	99.89	2.24
Step Length (mm)	60	60.04	61.88	60.31	99.55	2.61
Step Width (mm)	20	20.05	21.25	20.12	99.65	5.64
Step Depth (mm)	30	30.08	31.31	30.83	97.51	1.60
Hole Dia (mm)	10	9.93	9.43	9.57	96.37	1.41
Pocket 1 Dia (mm)	90	89.90	88.92	89.91	99.99	1.08
Pocket 2 Dia (mm)	60	59.85	58.43	59.94	99.85	2.22

Table 7 Multi-scan integration results

Workpieces	Number of Integrated Scans	Total Number of Frames	Max Registration Quality	Scanned Dimension Accuracy against CAD Dimensions (%)	Memory Storage (GB)	Scanning Time (mins)	Processing Time (mins)
Base Block	2 - AB	1849	0.200	99.30	2.256	3	10
	4–2A2B	3765	0.210	99.44	4.456	5	18
	8–4A4B	7312	0.205	99.75	8.396	8	23
Fixture	2 - AB	1971	0.400	98.47	2.250	3	6
	4–2A2B	3639	0.375	99.09	4.279	6	15
	8–4A4B	6762	0.3875	99.23	7.934	12	21
Fastener	2 - AB	2257	0.550	96.87	2.660	3	11
	4–2A2B	4314	0.550	97.09	5.150	5	18
	8–4A4B	7751	0.4875	98.58	9.325	10	25

4.4 Multi-scan integration

The impact of scan quantity on model accuracy was assessed by integrating two, four, and eight individual scans per workpiece, as shown in Table 7. Although increasing scan count enhanced surface completeness, improvements in dimensional accuracy were marginal—0.45%, 0.76%, and 1.15%, respectively. The maximum registration quality fluctuated, indicating that scan quality is more influential than scan quantity in determining overall accuracy. For instance, the base block achieved 99.30% accuracy with two scans and 99.75% with eight, yet memory usage increased from 2.26 GB to 8.40 GB, with corresponding scanning and processing times tripling. A similar trend was observed for the fixture and fastener models. This demonstrates a key industrial trade-off: while more scans can incrementally improve geometric fidelity, they impose significant costs in data storage, computation time, and workflow efficiency.

To assess the stability and reliability of the multi-scan integration process, the convergence behavior and residual errors of the iterative closest point (ICP) registration were analyzed for different numbers of scans. For each configuration, the mean point-to-point residual, standard deviation, and convergence iteration count were extracted from the registration logs.

The results indicate that the mean ICP residual decreased rapidly when increasing the number of scans from two to four, reflecting improved surface coverage and geometric redundancy. Beyond four scans, the reduction in residual error became marginal, with changes falling within the variability observed between repeated registrations. This suggests a diminishing return in registration accuracy as additional scans are introduced.

Convergence stability was evaluated by examining the number of iterations required to reach the stopping criterion. Registrations involving fewer than three scans exhibited higher variability in iteration count and occasional convergence to local minimum, particularly for asymmetric geometries. In contrast, configurations with four or more scans showed consistent convergence behavior, indicating improved robustness against initial alignment errors.

Orientation-dependent coverage analysis revealed that increasing scan count primarily enhanced data completeness in occluded regions and steep surface angles. However, excessive scan redundancy also increased overlap in already well-sampled regions, contributing to accumulated alignment uncertainty rather than measurable accuracy gains.

4.5 Positioning of the proposed workflow relative to existing denoising algorithms

The objective of this study is not to propose a novel denoising algorithm, nor to perform algorithmic optimization benchmarking. Instead, the primary research question concerns the controllability of noise in handheld structured-light scanning through acquisition-stage interventions and structured post-processing under realistic industrial constraints.

While classical filtering approaches such as Statistical Outlier Removal (SOR) and optimization-based techniques such as Moving Least Squares (MLS) have been extensively evaluated in prior literature, their reported performance is typically derived from static or synthetic datasets under controlled laboratory conditions. In contrast, this study focuses on noise behavior arising from handheld operation, reflective metallic surfaces, and geometric occlusion—conditions under which algorithmic performance may differ substantially from benchmark datasets.

Therefore, rather than re-implementing these algorithms for direct numerical comparison, the present work contextualizes its findings against reported performance characteristics in the literature. SOR is widely recognized for its efficiency in removing isolated outliers but limited capability in correcting structured or reflection-induced noise. MLS achieves strong surface smoothing performance but may introduce geometric shrinkage in high-curvature and recessed features.

The experimental results presented in Sect. 4.2–4.4 demonstrate that the majority of recoverable error originates during acquisition rather than post-processing. Once environmental stabilization, matte coating, and optimized scan trajectories were implemented, global smoothing yielded diminishing returns, particularly for small and recessed features. This behavior is consistent with the known limitations of global smoothing strategies reported in prior studies.

Accordingly, the contribution of this work should be interpreted as complementary rather than competitive to existing denoising algorithms. The proposed workflow emphasizes:

- Noise prevention over aggressive noise correction.
- Feature preservation over maximal surface smoothing.
- Industrial feasibility over computational optimality.

Future research may extend this work by integrating the proposed acquisition-stage controls with advanced denoising algorithms to evaluate potential cumulative benefits.

5 Discussion

From a scientific perspective, the contribution of this work differs from conventional denoising studies that prioritize maximal numerical error reduction. Instead, it demonstrates that under inspection-oriented constraints, the majority of recoverable error originates from acquisition-stage factors rather than post-processing alone. The experimental results show that once acquisition noise is controlled, further algorithmic smoothing yields diminishing returns and may compromise feature fidelity.

It is important to clarify that the absence of direct algorithmic benchmarking does not imply equivalence or superiority relative to SOR, MLS, or learning-based approaches. Rather, this study isolates a different dimension of the problem, the extent to which noise can be mitigated prior to algorithmic intervention. The results indicate that acquisition-stage stabilisation accounts for a substantial proportion of recoverable deviation, suggesting that algorithmic optimisation alone may not address the dominant sources of error in handheld structured-light inspection.

This insight provides an explanatory framework for understanding the limited effectiveness of advanced denoising algorithms in handheld inspection scenarios and highlights the importance of constraint-aware methodology design.

While Artec Studio 17 was selected for its industrial relevance and integration with the Artec Leo scanner, the observed trends in noise reduction and feature-dependent accuracy are not software-specific. The improvements achieved through matte surface treatment, controlled acquisition conditions, and neighbourhood-based filtering reflect fundamental properties of structured-light scanning and point cloud processing, rather than proprietary algorithm behaviour.

Conversely, the limited improvement observed for small and recessed features persisted across parameter variations, indicating that these errors are governed primarily by optical resolution, occlusion, and reflectivity effects rather than by post-processing software choice. This reinforces the interpretation that certain geometric inaccuracies represent irrecoverable information loss rather than insufficient filtering.

5.1 Findings in noise reduction process

The findings of this study demonstrate how handheld 3D scanning, when applied through an industry-oriented workflow, can yield consistent accuracy improvements in automated dimensional inspection. Although 3D scanning enables non-contact, high-resolution measurement, its effectiveness in industrial environments depends heavily on mitigating optical noise and optimising data processing.

The first stage of the workflow focused on pre-processing strategies, where applying a matte surface spray proved highly effective in suppressing reflectivity and outlier noise. While the coating adds minor preparation time and material cost, its benefits, particularly for glossy or metallic components, far outweigh the trade-offs in industrial settings. Customised scanning paths with overlapping passes and variable angles further improved coverage of occluded regions, enhancing the capture of small features. Manual handling remained a minor error source, as variation in operator motion introduced small deviations in repeated scans. Overall, Stage One improved dimensional accuracy by 1.03% relative to CAD models.

In Stage Two, a systematic post-processing workflow was developed in Artec Studio 17. The most effective parameters for outlier removal were identified as a 0.6 mm resolution and a noise level of three, balancing aggressive noise elimination with model integrity. A small-object filter with a 25% polygon threshold efficiently removed residual outliers without excessive data loss.

For surface refinement, smoothing algorithms played a key role in approximating true geometry. However, industrial users must consider trade-offs between accuracy and feature fidelity. Smooth fusion handled sparse point clouds effectively but tended to oversmooth edges and reduce definition in small or recessed features. In contrast, sharp fusion preserved corners and planar transitions but introduced minor dimensional shrinkage. Across all workpieces, smoothing improved overall dimensional accuracy by 1.76%, though small features such as threaded holes (84.8% accuracy) and notch depths (53.0%) remained challenging. Because Artec Studio 17 applies smoothing globally, future work should investigate localised or adaptive smoothing techniques that target specific surface regions to improve small-feature retention.

Multi-scan integration was evaluated to assess its influence on geometric consistency. The results showed that increasing scan count beyond four did not substantially enhance registration quality or accuracy, as scan quality had a greater impact than quantity. Integrating four scans offered the most practical trade-off, balancing improved dimensional accuracy, memory requirements, and processing time. Eight-scan integration only increased accuracy marginally (~ 1%) while tripling data storage and computation time, which is impractical for large-scale industrial workflows.

In summary, the key lessons for practitioners are:

- Matte coating effectively reduces reflectivity-induced noise, but requires additional preparation.
- Four scans represent the optimal balance between accuracy, resource usage, and processing time.
- Smooth vs. sharp fusion involves trade-offs.

These findings provide a validated reference for practitioners developing efficient, scalable 3D scanning workflows for industrial inspection.

5.2 Limitations in small-feature accuracy and physical interpretation

Although the proposed two-stage workflow achieved consistent improvements in overall dimensional accuracy (1–2%), the reconstruction accuracy of small geometric features, such as threaded holes, narrow notches, and blind cavities—remained comparatively low. This behaviour was observed consistently across all test components and was only marginally influenced by post-processing parameter variation. These findings indicate that the limited improvement in small-feature accuracy is not primarily attributable to insufficient denoising, but rather to fundamental physical and geometric constraints inherent to handheld structured-light scanning.

From an optical perspective, structured-light scanners rely on triangulation between a projected fringe pattern and camera sensors. When the characteristic size of a feature approaches the scanner's effective pixel footprint or projected fringe width, the captured signal becomes contrast-limited, leading to unstable correspondence and increased depth uncertainty. Previous studies have shown that depth noise increases sharply when feature dimensions fall below two to three times the system's lateral resolution, rendering such features highly sensitive to noise and smoothing artefacts.

In addition, small and recessed features are disproportionately affected by occlusion and shadowing effects. For threaded holes and blind cavities, portions of the projected pattern are partially or fully blocked, resulting in incomplete or asymmetric point sampling. This leads to systematic bias rather than random noise, which cannot be fully corrected through global smoothing or statistical filtering. As a result, post-processing operations may reduce surface roughness while simultaneously distorting feature geometry, explaining the observed reduction in notch depth and thread definition after smoothing.

Surface reflectivity further amplifies these limitations. Even with matte coating, residual specular components can cause multipath reflections near sharp edges and concave regions, producing ghost points that blur feature boundaries. Because these artefacts are spatially correlated with the feature geometry, aggressive filtering risks removing valid data, while conservative filtering leaves residual noise. This trade-off highlights the inherent difficulty of applying global denoising strategies to features with high curvature and limited visibility.

The limited absolute improvement observed for small features therefore reflects a transition from noise-dominated error to information-limited error. Once acquisition noise is reduced through environmental control and surface treatment, the remaining deviations are governed primarily by scanner resolution, optical geometry, and feature accessibility. Under these conditions, further global smoothing yields diminishing returns and may degrade metrological reliability.

These findings suggest that improving small-feature accuracy requires either localized, feature-aware denoising strategies or alternative acquisition approaches, such as higher-resolution scanners, multi-scale scanning, or complementary tactile measurement for critical features. Within the constraints of handheld structured-light systems, the proposed workflow achieves near-optimal performance for accessible features while clearly delineating the boundaries of achievable accuracy for fine geometries.

5.3 Reproducibility and software-independent parameterisation

Table 8 summarises the functional equivalence between the proprietary operations used in this study and their open-source counterparts, along with the corresponding parameter ranges. By explicitly reporting these parameters, the workflow can be replicated or extended using alternative software environments without reliance on Artec Studio.

This abstraction ensures that the scientific contribution of the work lies in the experimentally validated workflow and feature-dependent noise analysis, rather than in the use of any specific commercial software package.

Table 8 Functional equivalence between Artec Studio operations and open-source implementations

Processing Stage	Artec Studio 17	Open-source equivalent	Key parameters
Outlier Removal	Outlier filter	SOR (PCL / CloudCompare)	k-neighbours, $\sigma = 2–3$
Noise smoothing	Smooth fusion	MLS	Radius = 0.3–0.6 mm
Registration	Global registration	ICP	Max error, iterations

5.4 Generalizability and industrial applicability

Although the proposed workflow is motivated by industrial inspection practice, the experimental evaluation was performed under controlled conditions that do not fully represent the variability encountered in production environments. Factors such as fluctuating ambient lighting, mechanical vibration, temperature drift, surface contamination, and operator-dependent scanning strategies are known to influence structured-light measurement quality and were not explicitly varied in the present study.

Previous research has shown that optical 3D scanning accuracy can degrade significantly under non-ideal environmental conditions, particularly for handheld systems that rely on stable illumination and precise triangulation geometry. Variations in operator motion and scanning distance further introduce stochastic errors that are difficult to decouple from algorithmic noise reduction effects.

Within this context, the results presented in this work should be interpreted as demonstrating the potential accuracy gains achievable when acquisition-stage conditions are reasonably controlled. The observed improvements therefore represent an upper-bound performance envelope rather than a guaranteed outcome under all industrial scenarios.

Nevertheless, the structure of the proposed workflow remains applicable across a wide range of inspection environments, particularly the separation of acquisition-stage control and post-processing noise attenuation. While the magnitude of improvement may vary, the methodological insight that acquisition-stage factors dominate recoverable noise is expected to remain valid. Future work will focus on extending the evaluation to disturbed environments and multi-operator scenarios to assess robustness and repeatability.

5.5 Sustainability

Beyond accuracy improvements, the proposed workflow contributes to more sustainable manufacturing practices. By reducing measurement discrepancies, it directly minimises rework, scrap rates, and material waste, supporting UN Sustainable Development Goal (SDG) 12 – Responsible Consumption and Production. Optimised scan integration also reduces digital storage demands; even a 1 MB reduction in 3D data size lowers CO_2 emissions by approximately 15 g, reinforcing SDG 13 – Climate Action through digital carbon footprint reduction [17].

Digitising geometric measurement further promotes remote collaboration and reduced transport emissions, aligning with SDG 3 – Good Health and Well-being. Collectively, the two-stage methodology enhances the robustness of handheld 3D scanning in automated inspection systems, increasing manufacturing productivity and supporting SDG 9 – Industry, Innovation and Infrastructure [28].

Recent industrial initiatives such as Belfast City Council's £100 million investment in the Advanced Manufacturing Innovation Centre (AMIC) exemplify how enhanced digital inspection workflows can drive regional innovation and workforce development, creating high-value jobs and contributing to sustainable industrial growth.

6 Conclusion

This study developed and validated an industry-oriented, two-stage workflow for noise reduction in handheld 3D scanning, demonstrated through a case study on automated dimensional inspection. The proposed approach provides a practical framework for industry practitioners seeking to enhance scan accuracy, repeatability, and data reliability without requiring advanced computational expertise.

Stage One (pre-processing) focused on minimizing noise at the source through environmental control, surface preparation, and optimized scanning paths. By maintaining a stable laboratory environment (20 °C, 1200 lx illumination), applying a matte coating to reduce reflective noise, and using custom scan trajectories to improve coverage of occluded regions, dimensional accuracy improved by 1.03% relative to CAD reference models. Although the matte spray increased preparation time and marginally reduced some dimensional precision, it consistently reduced outliers and improved scan uniformity.

Stage Two (post-processing) established a robust Artec Studio 17 workflow integrating outlier removal (0.6 mm resolution, noise level = 3), small-object filtering (25% polygon threshold), and selective smoothing at 0.3 mm resolution to balance surface refinement with feature preservation. This process improved geometric accuracy by an additional 1.76%, though fine features such as threaded holes and chamfer edges remained susceptible to over-smoothing and minor geometric distortion.

Multi-scan integration analysis demonstrated that scan quality outweighed scan quantity in determining accuracy. While integrating additional scans (up to eight) yielded less than 2% improvement, it tripled memory requirements and processing time. The optimal industrial configuration involved four high-quality scans, achieving consistent alignment (maximum registration error < 0.3 mm) while maintaining efficient data management.

Collectively, the workflow achieved measurable improvements in dimensional accuracy—1.03% in pre-processing, 1.76% through smoothing, and 0.69% via multi-scan integration—while enhancing repeatability and sustainability in digital inspection. The reduction of measurement errors directly supports lower rework rates, reduced material waste, and improved resource efficiency, aligning with sustainable manufacturing practices.

The comparative benchmarking results highlight an important distinction between noise suppression capability and inspection suitability. The proposed workflow intentionally prioritizes stability, interpretability, and feature preservation over maximum numerical improvement. Within the constraints of handheld structured-light scanning, the observed 1–2% improvement represents a transition from noise-dominated error to resolution-limited error, beyond which further algorithmic processing yields diminishing or counterproductive returns. This positions the workflow as a complementary, rather than competing, approach to advanced denoising techniques.

The proposed two-stage workflow demonstrates measurable improvements in dimensional accuracy under controlled scanning conditions representative of best-practice industrial inspection. While the results cannot be directly generalized to all factory-floor environments, they provide a validated baseline that clarifies the relative contributions of acquisition-stage control and post-processing denoising. These findings offer guidance for practitioners seeking to maximize inspection reliability under constrained conditions and establish a foundation for future robustness-oriented studies.

Future work should extend this approach to a wider range of materials, surface finishes, and colours to further validate its robustness across industrial contexts. The integration of robotic scanning platforms could enhance repeatability by eliminating manual variation in distance and motion, while open-source tools such as CloudCompare offer promising opportunities for replicating and extending this workflow with customized, localized noise-reduction algorithms.

In summary, this research presents a replicable, industry-ready workflow that balances accuracy, sustainability, and practicality—offering a scalable foundation for the adoption of handheld 3D scanning in automated dimensional inspection and quality assurance environments.

Appendix

Table 9 Measurements of products

Name	Images
Digital callipers	
Fixture	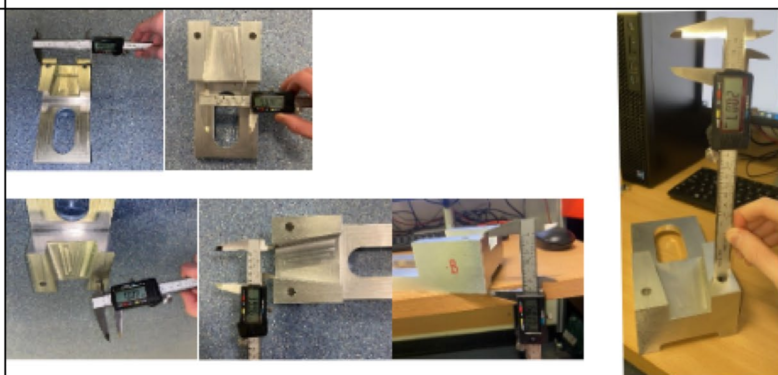
Fastener	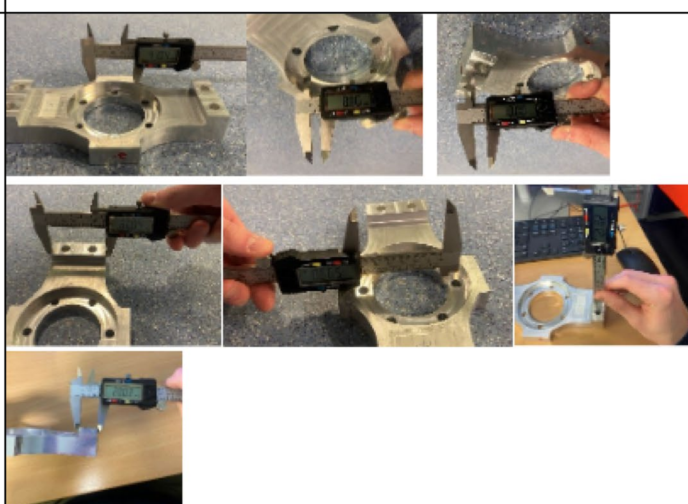
Based block	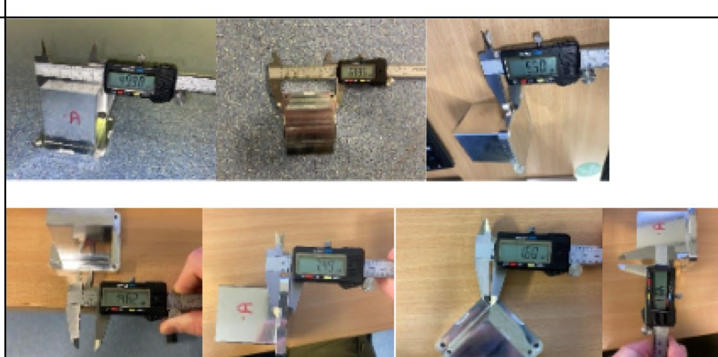

Appendix

Table 10 CAD drawings of products

Product	Drawing
Fixture	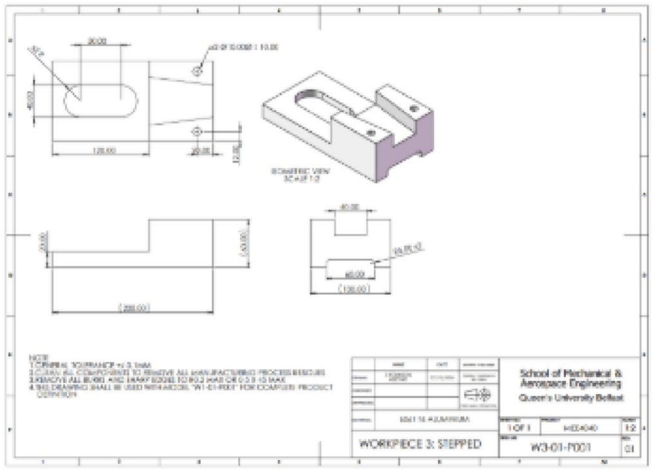
Fastener	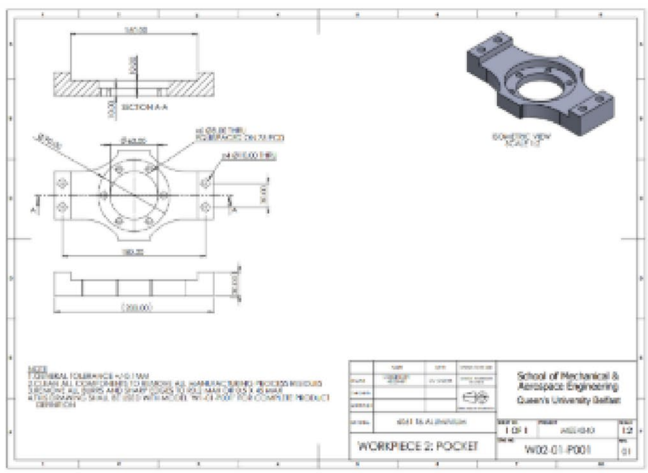
Based block	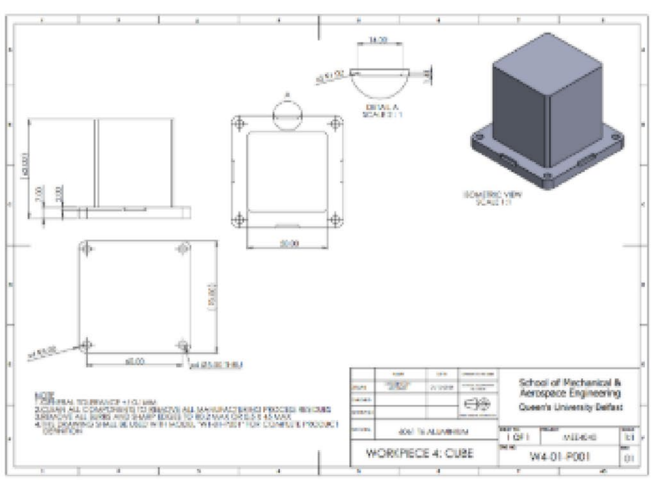

Appendix

Table 11 Pre-processing results

Dimension	Noise Identification (mm)	After Stage 1 (mm)	CAD (mm)	Accuracy Improvement against CAD (%)
Base Block				
Width 1 (mm)	50.14	50.14	50	0.00
Width 2 (mm)	50.64	50.18	50	0.92
Height (mm)	63.27	63.07	62.5	0.32
Height-Base (mm)	55.21	55.18	55	0.05
Base Depth (mm)	N/A	8.02	7.5	N/A
Thread Hole Dia (mm)	5.94	5.78	5	3.20
Notch Depth	N/A	N/A	2	N/A
Notch Length	N/A	N/A	15	N/A
Fixture				
Dimension	Noise Identification (mm)	After Stage 1 (mm)	CAD (mm)	Accuracy Improvement against CAD (%)
Width (mm)	101.25	100.50	100	0.75
Step Length (mm)	80.77	80.55	80	0.28
Step Depth (mm)	60.66	60.51	60	0.25
Hole Dia (mm)	9.49	9.45	10	-0.40
Hole Depth (mm)	N/A	N/A	5	N/A
Slot Width (mm)	38.94	39.67	40	1.83
Slot Length (mm)	88.61	88.50	90	-0.12
Groove Width (mm)	59.41	60.31	60	0.47
Groove Depth (mm)	10.85	10.73	10	1.20
Fastener				
Dimension	Noise Identification (mm)	After Stage 1 (mm)	CAD (mm)	Accuracy Improvement against CAD (%)
Width (mm)	115.03	112.83	112.5	1.96
Step Length (mm)	61.88	60.61	60	2.12
Step Width (mm)	21.25	20.42	20	4.15
Step Depth (mm)	31.31	31.06	30	0.83
0Hole Dia (mm)	9.43	9.52	10	0.90
Pocket 1 Dia (mm)	88.92	89.15	90	0.26
Pocket 2 Dia (mm)	58.43	60.16	60	2.35

Author Contributions All authors contributed to the study conception and design. Material preparation, data collection and analysis were performed by Scott Robinson and Chengsi Lin. The first draft of the manuscript was written by Scott Robinson, and major modified by Chengsi Lin, and all authors commented on previous versions of the manuscript. All authors read and approved the final manuscript.

Funding The authors declare that no funds, grants, or other support were received during the preparation of this manuscript.

Declarations

Competing Interests The authors have no relevant financial or non-financial interests to disclose.

References

1. Klyatis LM, Klyatis EL, PRACTICAL ACCELERATED QUALITY DEVELOPMENT AND INPROVEMENT IN, AND DESIGN, in (2006) In: MANUFACTURING (ed) Accelerated Quality and Reliability Solutions. Elsevier, pp 363–411. https://doi.org/10.1016/B978-008044924-1/50005-8.
2. Jadayel M, Khameneifar F (2024) Structured-light 3D Scanning Performance in Offline and In-process Measurement of 3D Printed Parts. Procedia CIRP 126:987–992. https://doi.org/10.1016/j.procir.2024.08.372
3. See JE, Drury CG, Speed A, Williams A, Khalandi N (2017) The Role of Visual Inspection in the 21 Century. Proc Hum Factors Ergon Soc Annual Meeting 61:262–266. https://doi.org/10.1177/1541931213601548
4. Wang W, Liu X, Zhou H, Wei L, Deng Z, Murshed M, Lu X (2024) Noise4Denoise: Leveraging noise for unsupervised point cloud denoising. Comput Vis Media (Beijing) 10:659–669. https://doi.org/10.1007/s41095-024-0423-3
5. Sun C, Shi J, Wang M, Ding J (2025) Method for Restoring point cloud information from complex reflective surface line structured light Scans. Opt Laser Technol 183:112316. https://doi.org/10.1016/j.optlastec.2024.112316
6. Frank AG, Dalenogare LS, Ayala NF (2019) Industry 4.0 technologies: Implementation patterns in manufacturing companies. Int J Prod Econ 210:15–26. https://doi.org/10.1016/j.ijpe.2019.01.004
7. Major M, Mészáros B, Würsching T, Polyák M, Kammerhofer G, Németh Z, Szabó G, Nagy K (2024) Evaluation of a Structured Light Scanner for 3D Facial Imaging: A Comparative Study with Direct Anthropometry. Sensors 24:5286. https://doi.org/10.3390/s24165286
8. Schipper JAM, Merema BJ, Hollander MHJ, Spijkervet FKL, Dijkstra PU, Jansma J, Schepers RH, Kraeima J (2024) Reliability and validity of handheld structured light scanners and a static stereophotogrammetry system in facial three-dimensional surface imaging. Sci Rep 14:8172. https://doi.org/10.1038/s41598-024-57370-x
9. Li T, Polette A, Lou R, Jubert M, Nozais D, Pernot J-P (2024) Machine learning-based 3D scan coverage prediction for smart-control applications. Comput Aided Des 176:103775. https://doi.org/10.1016/j.cad.2024.103775
10. Helle RH, Lemu HG (2021) A case study on use of 3D scanning for reverse engineering and quality control. Mater Today Proc 45:5255–5262. https://doi.org/10.1016/j.matpr.2021.01.828
11. Kuş A (2009) Implementation of 3D Optical Scanning Technology for Automotive Applications. Sensors 9:1967–1979. https://doi.org/10.3390/s90301967
12. Javaid M, Haleem A, Pratap Singh R, Suman R (2021) Industrial perspectives of 3D scanning: Features, roles and it's analytical

applications. Sens Int 2:100114. https://doi.org/10.1016/j.sintl.2021.100114
13. Edl M, Mizerák M, Trojan J (2018) 3D LASER SCANNERS: HISTORY AND APPLICATIONS. Acta Simulatio 4:1–5. https://doi.org/10.22306/asim.v4i4.54
14. Mitra S (2025) accessed December 18, What is structured light 3d scanning? Metrologically Speaking (n.d.). https://metrologicallyspeaking.com/what-is-structured-light-3d-scanning/
15. Jacobs L, Dvorak J, Cornelius A, Zameroski R, No T, Schmitz T (2023) Structured light scanning artifact-based performance study. Manuf Lett 35:873–882. https://doi.org/10.1016/j.mfglet.2023.07.014
16. Li F, Stoddart D, Zwierzak I (2017) A Performance Test for a Fringe Projection Scanner in Various Ambient Light Conditions. Procedia CIRP 62:400–404. https://doi.org/10.1016/j.procir.2016.06.080
17. Cutti AG, Santi MG, Hansen AH, Fatone S (2024) Accuracy, Repeatability, and Reproducibility of a Hand-Held Structured-Light 3D Scanner across Multi-Site Settings in Lower Limb Prosthetics. Sensors 24:2350. https://doi.org/10.3390/s24072350
18. Mian NS, Fletcher S, Longstaff AP (2019) Reducing the latency between machining and measurement using FEA to predict thermal transient effects on CMM measurement. Measurement 135:260–277. https://doi.org/10.1016/j.measurement.2018.11.034
19. Ding S, Chen X, Ai C, Wang J, Yang H (2024) A noise-reduction algorithm for raw 3D point cloud data of asphalt pavement surface texture. Sci Rep 14:16633. https://doi.org/10.1038/s41598-024-65233-8
20. Luijten G, Gsaxner C, Li J, Pepe A, Ambigapathy N, Kim M, Chen X, Kleesiek J, Hölzle F, Puladi B, Egger J (2023) 3D surgical instrument collection for computer vision and extended reality. Sci Data 10:796. https://doi.org/10.1038/s41597-023-02684-0
21. Sun C, Miao L, Wang M, Shi J, Ding J (2023) Research on point cloud hole filling and 3D reconstruction in reflective area. Sci Rep 13:18524. https://doi.org/10.1038/s41598-023-45648-5
22. Chen H, Shen J (2018) Denoising of point cloud data for computer-aided design, engineering, and manufacturing. Eng Comput 34:523–541. https://doi.org/10.1007/s00366-017-0556-4
23. Palousek D, Omasta M, Koutny D, Bednar J, Koutecky T, Dokoupil F (2015) Effect of matte coating on 3D optical measurement accuracy. Opt Mater (Amst) 40:1–9. https://doi.org/10.1016/j.optmat.2014.11.020
24. Wang Y, Feng H-Y (2014) Modeling outlier formation in scanning reflective surfaces using a laser stripe scanner. Measurement 57:108–121. https://doi.org/10.1016/j.measurement.2014.08.010
25. Reichard CA (2020) Test and Evaluation of an Artec Leo 3D Scanner. https://repository.fit.edu/etd
26. Trucco E, Fisher RB, Fitzgibbon AW Direct Calibraction and Data Consistency in 3-D Laser Scanning, in: British Machine Vision Association and Society for Pattern Recognition, 2013: p. 48.1–48.10. https://doi.org/10.5244/c.8.48
27. Sun X, Rosin PL, Martin RR, Langbein FC (2009) Noise analysis and synthesis for 3D laser depth scanners. Graph Models 71:34–48. https://doi.org/10.1016/j.gmod.2008.12.002
28. Denayer M, De Winter J, Bernardes E, Vanderborght B, Verstraten T (2024) Comparison of Point Cloud Registration Techniques on Scanned Physical Objects. Sensors 24:2142. https://doi.org/10.3390/s24072142
29. Wang X, Fan X, Zhao D (2023) PointFilterNet: A Filtering Network for Point Cloud Denoising. IEEE Trans Circuits Syst Video Technol 33:1276–1290. https://doi.org/10.1109/TCSVT.2022.3207789
30. Radu Bogdan Rusu N, Blodow Z, Marton A, Soos M, Beetz (2007) Towards 3D object maps for autonomous household robots, in: 2007 IEEE/RSJ International Conference on Intelligent Robots and Systems, IEEE, : pp. 3191–3198. https://doi.org/10.1109/IROS.2007.4399309
31. Pirotti F, Ravanelli R, Fissore F, Masiero A (2018) Implementation and assessment of two density-based outlier detection methods over large spatial point clouds. Open Geospatial Data Softw Stand 3:14. https://doi.org/10.1186/s40965-018-0056-5
32. Tomasi C, Manduchi R, Bilateral filtering for gray and color images, in: Sixth International Conference on Computer Vision (IEEE Cat. No.98CH36271), House NP n.d.: pp. 839–846. https://doi.org/10.1109/ICCV.1998.710815
33. Ullah B, Trevelyan J, Matthews PC (2014) Structural optimisation based on the boundary element and level set methods. Comput Struct 137:14–30. https://doi.org/10.1016/j.compstruc.2014.01.004
34. Mehrabi H, Voosoghi B (2015) Recursive moving least squares. Eng Anal Bound Elem 58:119–128. https://doi.org/10.1016/j.enganabound.2015.04.001
35. Xu Z, Foi A (2021) Anisotropic Denoising of 3D Point Clouds by Aggregation of Multiple Surface-Adaptive Estimates. IEEE Trans Vis Comput Graph 27:2851–2868. https://doi.org/10.1109/TVCG.2019.2959761
36. Charles RQ, Su H, Kaichun M, Guibas LJ, PointNet: Deep Learning on Point Sets for 3D Classification and Segmentation, in: IEEE Conference on Computer, Vision, Recognition P (2017) (CVPR), IEEE, 2017: pp. 77–85. https://doi.org/10.1109/CVPR.2017.16
37. Rakotosaona M, La Barbera V, Guerrero P, Mitra NJ, Ovsjanikov M (2020) PointCleanNet: Learning to Denoise and Remove Outliers from Dense Point Clouds. Comput Graphics Forum 39:185–203. https://doi.org/10.1111/cgf.13753
38. Chua CK, Wong CH, Yeong WY (2017) Software and Data Format. Standards, Quality Control, and Measurement Sciences in 3D Printing and Additive Manufacturing. Elsevier, pp 75–94. https://doi.org/10.1016/B978-0-12-813489-4.00004-0.
39. Berger M, Tagliasacchi A, Seversky L, Alliez P, Levine J, Sharf A, Silva C, Seversky LM, Levine JA, Silva CT (2014) State of the Art in Surface Reconstruction from Point Clouds. 161–185. https://doi.org/10.2312/egst.20141040ï
40. Hu X, Wei X, Sun J (2023) A Noising-Denoising Framework for Point Cloud Upsampling via Normalizing Flows. Pattern Recognit 140:109569. https://doi.org/10.1016/j.patcog.2023.109569